Eur. Phys. J. E (2015) **38**: 50
DOI 10.1140/epje/i2015-15050-3

THE EUROPEAN PHYSICAL JOURNAL E

Regular Article

A single charge in the actin binding domain of fascin can independently tune the linear and non-linear response of an actin bundle network*

M. Maier[1], K.W. Müller[2], C. Heussinger[3], S. Köhler[4], W.A. Wall[2], A.R. Bausch[1], and O. Lieleg[5,a]

[1] Lehrstuhl für Zellbiophysik E27, Physik-Department, Technische Universität München, Garching, Germany
[2] Institute for Computational Mechanics, Department of Mechanical Engineering, Technische Universität München, Garching, Germany
[3] Institute for Theoretical Physics, Universität Göttingen, Göttingen, Germany
[4] Department of Molecular and Cell Biology, University of California, Berkeley, CA, USA
[5] Institute of Medical Engineering IMETUM and Department of Mechanical Engineering, Technische Universität München, Garching, Germany

Received 23 January 2015 and Received in final form 12 March 2015
Published online: 27 May 2015

Abstract. Actin binding proteins (ABPs) not only set the structure of actin filament assemblies but also mediate the frequency-dependent viscoelastic moduli of cross-linked and bundled actin networks. Point mutations in the actin binding domain of those ABPs can tune the association and dissociation dynamics of the actin/ABP bond and thus modulate the network mechanics both in the linear and non-linear response regime. We here demonstrate how the exchange of a single charged amino acid in the actin binding domain of the ABP fascin triggers such a modulation of the network rheology. Whereas the overall structure of the bundle networks is conserved, the transition point from strain-hardening to strain-weakening sensitively depends on the cross-linker off-rate and the applied shear rate. Our experimental results are consistent both with numerical simulations of a cross-linked bundle network and a theoretical description of the bundle network mechanics which is based on non-affine bending deformations and force-dependent cross-link dynamics.

Introduction

Cells rely on spatially and temporally highly orchestrated assemblies of semi-flexible filaments to control and adapt their local mechanical properties [1]. Actin filaments are a key component in the cellular toolbox as they can be organized into networks with different morphologies and thus different viscoelastic properties [2–5]. A prominent example of such an actin filament structure is given by filopodia —hair-like protuberances in migrating cells in which the actin filaments are ordered into bundles. The dynamics and mechanics of filopodia are essential for the guidance of cellular movement, and cells make use of filopodia to sense external mechanical cues [6]. The ordered microarchitecture of filopodia is achieved by the cross-linking protein fascin [7,8], which organizes actin filaments into stiff, polar bundles with a hexagonal structure [9–11]. Fascin also plays an important role in cancer cell invasion [12,13] and locates in invadopodia [14,15]. The activity of fascin is regulated by a phosphorylation site which is located in both actin binding pockets of the cross-linker, and an additional regulation can occur via a C-terminal serine residue [16]. The actin-binding domain 1 (ABD1) is described as a MARCKS sequence containing a phosphorylation site and three lysine residues [17]. *In vivo* and *in vitro* studies on fascin mutations have shown reduced numbers of filopodia for a phospho-mimicking mutant S39E [18]. The actin-binding domain 2 (ABD2) has recently been determined by electron microscopy and mutational studies [19,20]. Selected point mutations in the ABD2 of fascin such as the R271E, K353E and K358E mutations prevent bundle formation, and the number of filopodia is reduced in mouse melanoma cells [19]. However, a detailed understanding how the exchange of a single amino acid in one of the actin binding domains of an actin cross-linking protein will affect the architecture and mechanical properties of the ensuing actin assembly is still missing.

* Supplementary material in the form of a .pdf file available from the Journal web page at
http://dx.doi.org/10.1140/epje/i2015-15050-3

[a] e-mail: oliver.lieleg@tum.de

Here, we demonstrate how selected point mutations in the binding site of the cross-linker fascin can independently tune the linear and non-linear response of a cross-linked actin bundle network. Whereas ensuing changes in the binding affinity of the mutant fascin molecules shift the absolute value of the network plateau modulus, alterations in the cross-linker off-rate induce a transition from strain-hardening to strain weakening in the non-linear response regime. Numerical simulations of bundle networks with different cross-linker off-rates reveal a linear phase boundary between network stiffening and hardening. This is consistent with a theoretical description of the non-linear network mechanics based on non-affine bending deformations of the network polymers and force-dependent unbinding of inter-bundle cross-links.

Methods

For reconstituting actin networks, G-actin is obtained from rabbit skeletal muscle and stored in lyophilized form at 21 °C [21]. The lyophilized actin is dissolved in deionized water and dialyzed against G-buffer (2 mM Tris, 0.2 mM adenosine triphosphate (ATP), 0.2 mM $CaCl_2$, 0.2 mM dithiothreitol (DTT), and 0.005% NaN_3; *p*H 8) at 4 °C and the G-actin solutions are kept at 4 °C and used within 7 days of preparation. Recombinant human fascin (55 kD) was prepared by a modification of the method of [17] as described by [22]. Fascin mutants are created by using a QuikChange site-directed mutagenesis kit (Agilent Technologies, Santa Clara, CA) and confirmed by DNA sequencing. The mutant fascin was expressed and purified in the same manner as the wild type. In the experiments, the molar ratio R between fascin and actin, $R = c_{\mathrm{fascin}}/c_{\mathrm{actin}}$, is tuned. The effective molar ratio is calculated according to the formula $R^* = \frac{1}{2}[(1 + R + \frac{K_D}{c_{\mathrm{actin}}}) - ((1 + R + \frac{K_D}{c_{\mathrm{actin}}})^2 - 4R)^{\frac{1}{2}}]$ as in [10]. Rheological measurements were performed on a stress-controlled rheometer (Physica MCR 301, Anton Paar, Graz, Austria) using a 50 mm plate-plate geometry and 160 μm plate separation. Frequency spectra are obtained in a strain-controlled mode using small strain amplitudes that correspond to torques in the range of 0.5 μN m, which ensures linear response. For probing the non-linear network response, transient shear experiments with constant shear rates $\mathrm{d}\gamma/\mathrm{d}t$ are used. As described before [23], the stress-strain relation obtained from those shear measurements is smoothed with a spline, interpolated and then numerically differentiated to obtain the tangent modulus $K = \mathrm{d}\sigma/\mathrm{d}\gamma$. To resolve the structure of actin-fascin networks, actin is polymerized in F-buffer (2 mM Tris, 2 mM MgCl2, 0.2 mM CaCl2, 0.2 mM DTT, 100 mM KCl, and 0.5 mM ATP; *p*H 7.5). For fluorescence microscopy filaments are stabilized with alexa488-phalloidin (life technologies, Darmstadt, Germany). Epi-fluorescence pictures were acquired on an Axiovert 200 microscope (Zeiss, Oberkochen, Germany) with a 100x objective (Zeiss) and captured with an Orca ER digital camera (Hamamatsu, Hamamatsu City, Japan).

Simulations are carried out using a Brownian dynamics finite element approach [24,25], which has already been applied to study the self-assembly of semi-flexible biopolymer networks [26] and the linear rheology of bundle networks [27]. In this approach, filaments and cross-linker molecules are discretized with non-linear, geometrically exact, three-dimensional Simo-Reissner beam elements. The beam formulation accounts for deformations resulting from axial extension, torsion, bending, and shear, and has been shown to reliably reproduce key dynamic properties of filaments [28,29]. Both filaments and cross-linkers are subject to stochastic forces and the viscous effects of the surrounding fluid, thus performing Brownian motion. Stochastic excitations are modeled by piece-wise constant increments of a standard Wiener process in three dimensions. Viscous effects are accounted for by an effective velocity-dependent, anisotropic friction model [24]. A total number of $N_{\mathrm{f}} = 360$ filaments of length $l_{\mathrm{f}} = 4\,\mu$m and $N_{\mathrm{l}} = 9000$ initially free and explicitly modeled cross-linker molecules (molar ratio of $R \approx 0.02$) are placed into a cubic confinement of edge length $H = 6\,\mu$m, which is equipped with periodic boundary conditions. The persistence length of the filaments is $l_{\mathrm{p}} \sim 10\,\mu$m. The stiffness of a linker molecule is set to $k_x = 0.122\,$pN/nm and its average length to $l_x = 100\,$nm. The two species interact chemically and establish transient bonds, whose formation and breakup are governed by Poisson processes with the rate constants k_{on} and k_{off}, respectively. The off-rate k_{off} is force dependent and follows the Bell model [30]. The process of network simulation is divided into two stages. During the first stage, a network sample is generated by simulating the network evolution for $\sim 1000\,$s at a time step of $\Delta t = 0.01\,$s. The network exclusively consists of bundles at this point. Then a linear strain ramp is applied with a peak strain $\gamma = 25\%$ at different rates $\mathrm{d}\gamma/\mathrm{d}t$ to the top of the network and the averaged stresses are measured there.

Results

When added to actin filaments, wild type (WT) fascin forms purely bundled actin networks with straight, stiff bundles (fig. 1) at high molar ratios $R = c_{\mathrm{fascin}}/c_{\mathrm{actin}} > 0.01$. This bundling transition is accompanied by a strong increase in the network shear modulus [31]. A very similar network microstructure is observed when the point mutations S357E or K358M, respectively, are induced in the C-terminal actin binding pocket of fascin (fig. 1b and c).

Accordingly, the viscoelastic properties of all those networks should be similar as well. Indeed, in the linear response regime, the frequency spectra of all actin/fascin networks have very similar shapes (see inset of fig. 2). Moreover, the K358M mutant network also exhibits a similar dependence of the plateau modulus G_0 on the actin/fascin ratio R as observed for WT fascin. In detail, we find a structural and rheological transition point at $R \sim 0.01$ which agrees very well with the bundling transition observed for WT fascin [32]. This suggests that this fascin mutant has a similar binding affinity towards

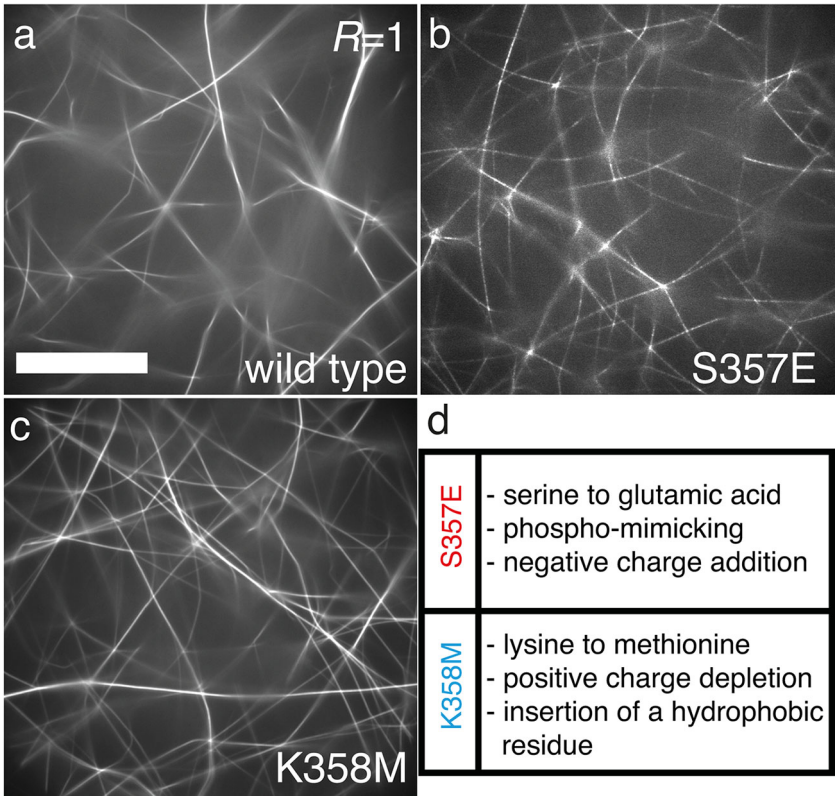

Fig. 1. Fluorescence micrographs of actin-fascin networks for 0.13 mg/mL actin, $R = c_{\mathrm{fascin}}/c_{\mathrm{actin}} = 1$. The scale bar represents 3 μm and applies to all images. A typical network formed by wild type fascin is depicted in (a), actin/fascin networks with mutations in the second actin-binding domain of fascin are shown in (b) for the S357E mutant and in (c) for the K358M mutant. The details of each point mutation are listed in (d).

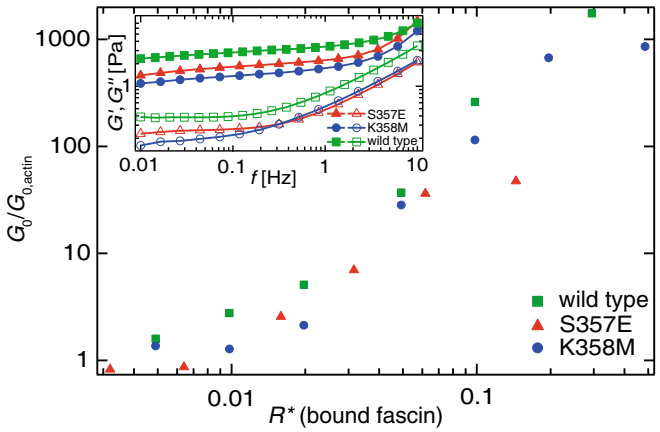

Fig. 2. The plateau modulus G_0 of bundled actin/fascin networks is normalized by the plateau modulus of an entangled actin solution and shown as a function of the effective molar ratio R^* of bound fascin. Data sets obtained for WT fascin as well as for the K358M and S357E mutants all collapse onto a single master relation. The original frequency spectra for 0.4 mg/mL actin and an effective $R^*_{\mathrm{WT}} = R^*_{\mathrm{K358M}} = R^*_{\mathrm{S357E}} = 0.05$ are shown in the inset.

actin as WT fascin. When normalizing both data sets by plotting the plateau moduli as a function of bound fascin, $R^* = c_{\mathrm{fascin,\,bound}}/c_{\mathrm{actin}}$, and assuming an identical binding affinity of $K_D = 20\,\mu$M [17] for WT fascin and the K358M mutant, both curves align (fig. 2). In contrast, for the S357E mutant, the rheological transition occurs at a higher molar ratio of $R \sim 0.1$. The S357E mutant is supposed to mimic a phosphorylated form of fascin at the C-terminal binding domain similar to the S39E mutant of the N-terminal binding domain. A reduced binding affinity has been described for the the naturally occurring phosphorylated form of fascin [17]. Thus, it is reasonable to assume that the binding affinity of this mutant might resemble that of phosphorylated fascin. Indeed, when S357E data is normalized as well using the binding affinity of phosphorylated fascin, this data set also collapses onto the WT fascin data (fig. 2).

It is somewhat surprising that the K_D value from a fully phosphorylated fascin variant [17] can be used for our phospho-mimicking fascin mutant which is only modified at one actin binding domain. However, the success of this procedure seems to justify our approach. The successful renormalization of the data suggests that the phospho-mimicking S357E mutation has altered the binding affinity of the fascin molecule towards actin whereas the K358M mutation has not. In the non-linear response regime, WT fascin/actin bundle networks exhibit a tunable behavior ranging from strain-hardening to strain-weakening [32]. One critical parameter setting the type of non-linear response is the shear rate $\mathrm{d}\gamma/\mathrm{d}t$ (fig. 3a).

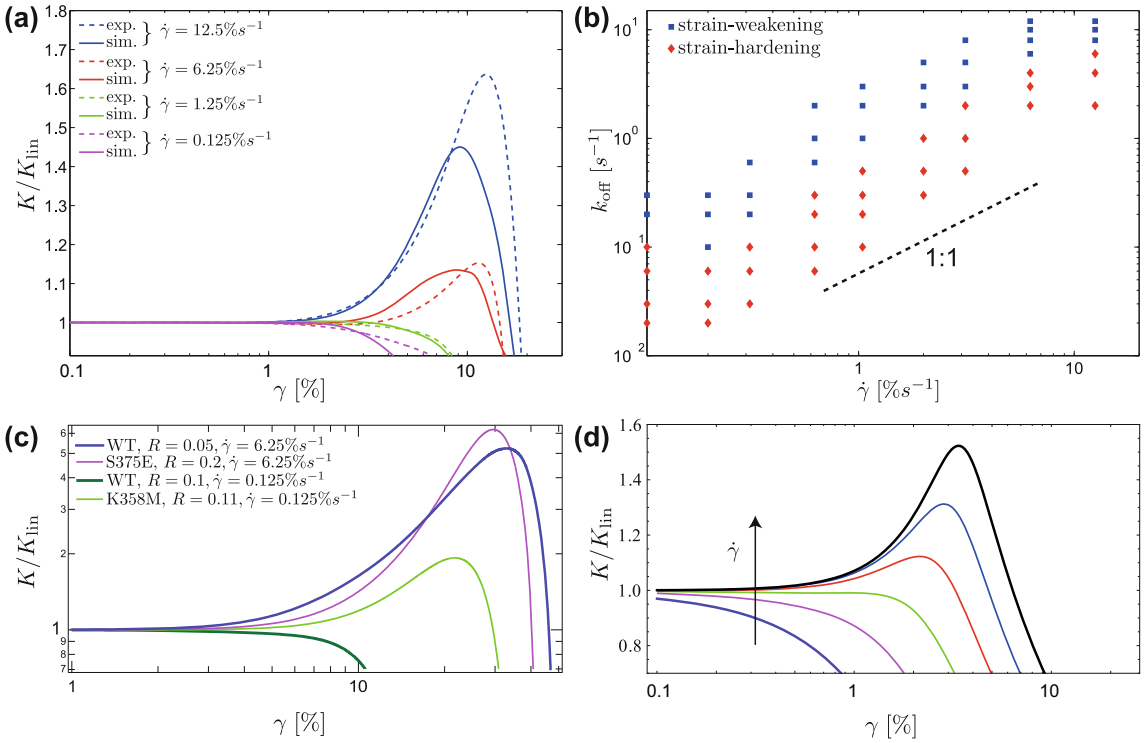

Fig. 3. Non-linear response of actin bundle networks. (a) Comparison of experimental and numerical response of a WT fascin/actin bundle network with $R \sim 0.1$. The differential modulus $K = \mathrm{d}\sigma/\mathrm{d}\gamma$ is shown for different shear rates. (b) Phase diagram of the weakening-to-hardening transition of simulated actin bundle networks. At the phase boundary, a roughly linear relation between the cross-linker off-rate and the shear rate is observed. (c) Differential modulus K normalized by its value in the linear regime as a function of strain at different shear rates ($\mathrm{d}\gamma/\mathrm{d}t = 0.125\%/\mathrm{s}$, $6.25\%/\mathrm{s}$) for actin bundle networks formed by wild-type fascin and fascin mutants S357E and K358M, respectively. (d) Calculated non-linear response of a cross-linked bundle network which is exposed to different strain rates. In this model, the bundles are connected via n crosslinks and the cross-link dynamics is described by rate equations (see main text for details).

In this non-linear regime, the network response is thought to be sensitive to the cross-linker off-rate as force-induced cross-linker unbinding between individual bundles dictates whether shear-hardening can be evoked or not [32–34]. When the cross-linker concentration in fascin mutant networks is chosen such that the linear network response matches that of a WT fascin/actin network, this does not necessarily have to be true for the non-linear behavior as well. However, this is the case for the phospho-mimicking S357E mutant. Here, both the onset of non-linear behavior as well as the maximum in the tangent modulus $K = \mathrm{d}\sigma/\mathrm{d}\gamma$ agree well with the corresponding values of the WT fascin/actin network (fig. 3c). In contrast, for the K358M fascin mutant, networks with matching linear viscoelastic response spectra exhibit markedly different non-linear responses than the corresponding WT fascin/actin network: the mutant network shows strain-hardening whereas the WT network exhibits strain-weakening at a low shear rate of $\dot\gamma = 0.125\%/\mathrm{s}^{-1}$ (fig. 3c). As the mechanical stability of a transient bundle-bundle cross-link is thought to determine the degree of network stiffening, we hypothesize that the qualitative difference observed for the mutant network is due to a reduced off-rate in the K358M fascin as the cross-links would need to be more stable as for WT fascin to allow for strain hardening at an identical shear rate.

To test this hypothesis, we employ a Brownian dynamics finite element approach, which correctly reproduces the linear viscoelastic frequency response of actin networks bundled by WT fascin [27]. Also for the non-linear response of the bundle network, we find very good agreement between our numerical simulations and the experimental data. The onset of non-linearity as well as the type and strength of the non-linear response are correctly returned by the simulation (fig. 3a) when a comparable fascin/actin ratio is used for generating the network morphology *in silico*. Probing the non-linear response of a given bundle network geometry with a fixed off-rate $k_{\rm off} = \text{const.}$ yields a transition from hardening to weakening with decreasing shear rate $\mathrm{d}\gamma/\mathrm{d}t$ as depicted in fig. 3a. Vice versa, vertical paths through the phase space, *i.e.* when $\mathrm{d}\gamma/\mathrm{d}t$ is held constant and the off-rate is varied, return a similar transition from hardening to weakening with increasing $k_{\rm off}$. This interplay between the shear rate and the cross-linker off-rate has already been suggested [32], yet direct experimental evidence has to date been lacking. Probing a broad range of cross-linker off-rates and shear rates, we obtain a phase diagram (fig. 3b) with a clear phase boundary marking the transition from strain-

hardening to strain-weakening. This phase boundary appears to follow a linear relation $\mathrm{d}\gamma/\mathrm{d}t \sim k_{\mathrm{off}}$ which suggests that a simple theoretical model considering both the bending and stretching energy of actin bundles as well as the force-dependent life-time of interconnecting cross-links might be able to reproduce this behavior.

To set up such a description, we build on a model that has successfully been used to explain the linear rheology of bundled actin-fascin networks [31,35]. Related models have been proposed in [36,37]. The general idea in our theoretical description is that, under large strain γ, two processes compete: first, non-linear filament elasticity beyond a strain γ_{c} leads to strain-stiffening; second, cross-link unbinding (at a rate k_{off}) leads to an increase in the wavelength λ of the bending modes and subsequently to strain-softening [36,38]. It is this interplay between the strain-scale γ_{c} and the time-scale $1/k_{\mathrm{off}}$ that can generate a transition from stiffening to weakening as the strain rate $\dot{\gamma}$ is varied (see fig. 3d).

In our model, network strain translates into non-affine filament bending deformations whose wavelengths λ are set by the typical inter-crosslink distances. We consider a filament of length L connected via n cross-links to the network. A strain ramp is applied to the network, *i.e.*, the strain increases linearly in time, $\gamma(t) = \dot{\gamma} \cdot t$. In response to the network strain, the filament starts to bend on the wavelength $\lambda = L/n$ set by the length of segments, *i.e.*, the distance between cross-links along the filament backbone. The amplitude of the bends $u_\perp = \gamma(t) \cdot L$ grows linearly with strain and is proportional to a constant length scale L, *e.g.*, the filament length [31,39]. If the bending amplitude is large enough, also longitudinal deformations follow, $u_\parallel \sim u_\perp^2/\lambda \sim \gamma^2 L^2/\lambda$, as governed by Pythagoras' law. Now, we additionally assume that cross-links can unbind such that the number of bound cross-links n decreases with time (neglecting rebinding). Thus, the bending wavelength gets longer, as $\lambda = L/n$, and the energy decreases. The interplay between stiffening and softening is then a competition between elastic stiffening (embodied in the non-linear longitudinal response) and softening via unbinding. To implement the softening part, we need a model for the elastic energy as well as a dynamical evolution equation for the cross-link number $n(t)$.

The bending energy of the filament is

$$E_{\mathrm{b}} = n k_\perp u_\perp^2 n^4 \gamma^2, \tag{1}$$

where we have used the bending spring constant $k_\perp \sim \kappa/\lambda^3$ of an elastic filament with the bending stiffness κ. The simplest form for the stretching energy would be to take just the linear response of a wormlike chain to longitudinal forces, characterized by a spring constant $k_\parallel \sim \kappa l_{\mathrm{p}}/\lambda^4$ and the persistence length l_{p}. Then

$$E_s = n k_\parallel u_\parallel^2 \sim n^7 \gamma^4. \tag{2}$$

The total energy then is $E = E_{\mathrm{b}} + E_{\mathrm{s}}$, the force F is the first derivative, the modulus μ is the second derivative with respect to strain

$$\mu \sim 2n^4(1 + 6n^3\gamma^2 l_{\mathrm{p}}). \tag{3}$$

Without cross-link unbinding, this describes a strain-stiffening system. The strain-dependence in the non-linear regime $\mu \sim \gamma^2$ follows from the assumption of linear longitudinal response and will be different, for example, when one considers the full non-linear force-extension relation of the wormlike chain or an exponential stiffening as in [36].

The simplest description for the cross-link dynamics is in terms of the rate equation

$$\frac{\mathrm{d}}{\mathrm{d}t} n = f(n) + b(n), \tag{4}$$

with forward rate f and backward rate b. Neglecting rebinding, $b = 0$. Unbinding happens at any one of n cross-links, thus $f = n \cdot k_{\mathrm{off}}$, with an off-rate that may be force dependent, $k_{\mathrm{off}} = k_0 \cdot e^{\frac{F}{F_0}}$, with the force F as given above. Solving the combined problem and substituting into the equation for the modulus μ then gives the curves in fig. 3d. Furthermore, the phase boundary between stiffening and weakening is then given by the condition $\gamma/\dot{\gamma} \sim 1/k_{\mathrm{off}}$, which implies $\dot{\gamma} \sim k_{\mathrm{off}}$, in agreement with the simulations.

Discussion

Point mutations in the actin binding domain of cross-linking and bundling ABPs are a useful tool to gain more insight into the structure-function-relationship of actin networks. In the actin bundling protein alpha-actinin, replacing the amino acid lysine (K) by glutamic acid (E) increases the binding affinity of the cross-linker towards actin and thus shifts the shear stiffness of the bundle network to higher values [40]. However, in that particular scenario, a third binding site of the cross-linker is activated by the point mutation, which is a completely different scenario from what we describe here. Our data suggests that the fascin mutant S357E has a reduced binding affinity but identical off-rate compared to WT fascin. This implies that the on-rate of this fascin variant must be lowered compared to WT fascin. This assumption is consistent with the introduction of an additional negative charge into the actin binding pocket of fascin by replacing serine with glutamic acid: this should lead to increased repulsion between the cross-linker and the negatively charged actin and thus manifest itself in slowed-down kinetics of the association process. In contrast, the K358M mutant seems to possess a similar binding affinity as WT fascin but a reduced off-rate. This is consistent with the mutation here by introducing the amino acid methionine: this may increase the local hydrophobicity of the binding pocket, thus giving rise to a short-ranged attraction that mainly influences the dissociation process of the bond. However, to allow for an unchanged binding affinity, also the on-rate would have to be reduced in such a scenario. This picture agrees with the molecular exchange achieved by our point mutation: the K358M mutation has removed a positive charge from the actin binding pocket of fascin which may lead to a weakened long-range attraction between actin and fascin thus slowing down the association process. The point mutations discussed here have both been generated in the C-terminal

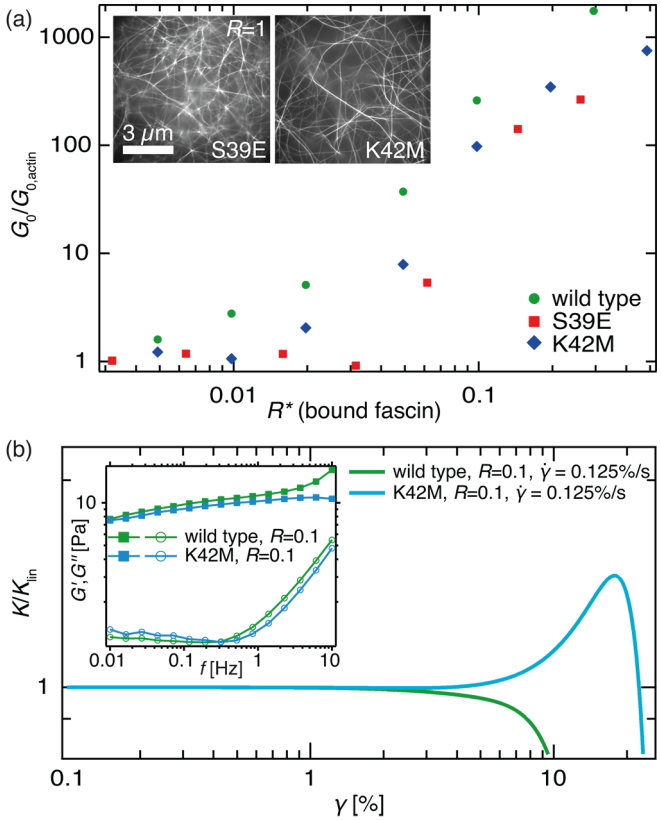

Fig. 4. Analogous mutations in the N-terminal actin binding pocket of fascin lead to similar rheological alterations as discussed for the C-terminal actin binding domain. (a) Plateau modulus G_0 normalized by the plateau modulus G_0 of an uncross-linked actin solution, plotted as a function of the effective molar ratio R^* of bound fascin. Here, mutations are in the N-terminal actin-binding domain of fascin. Also for those mutants, purely bundled networks are observed (see inset). As for the mutations of the second binding domain discussed in the main text, the data for the fascin mutants collapses onto the WT data when the changes in the binding affinity are considered by calculating the ratio of effectively bound fascin. (b) The differential modulus K is normalized by its value in the linear regime and shown as a function of strain at a shear rate of $\mathrm{d}\gamma/\mathrm{d}t = 0.125\%/\mathrm{s}$ for wild type fascin and the fascin mutant K42M. The linear frequency spectra of both networks are virtually identical, yet the non-linear response is qualitatively different. These results agree with what we describe for the K358M mutant in the C-terminal binding site of fascin.

binding pocket of fascin. However, analogous point mutations in the N-terminal actin binding pocket of fascin lead to identical rheological behavior (see fig. 4), which underscores our findings. *In vivo*, the S39E mutant shows a fast dissociation from actin bundles and leads to less frequent occurrence of filopodia [18]. Our rheological data shows that both phospho-mimicking mutants, S357E and S39E, need to be present in a higher total concentration to achieve a similar proportion of bound fascin. Only then networks with comparable microarchitecture and elasticity as WT fascin networks are generated.

Thus, those two mutants are probably less suitable to provide networks with the necessary stiffness to push the cell membrane, which agrees with the *in vivo* observation. Further studies on fascin mutant networks with simultaneous mutations at both actin binding sites may provide even more detailed insights into the functionality of this cross-linker, but will require simulations with even higher complexity.

In conclusion, we have shown that the exchange of a single charged amino acid in the actin binding pocket of a cross-linker such as fascin can have far reaching consequences on the rheology of the network as both the linear as well as the non-linear network response sensitively depend on the on- and off-rates that set the transient bond between individual network constituents. We have argued that such alterations of the cross-linker on- and off-rates are consistent with the insertion or depletion of charge in the actin binding pocket of fascin. Of course, an amino acid exchange in this binding pocket could also lead to increased or reduced steric hindrance with actin during the binding process and thus influence the cross-linker binding dynamics geometrically. In any case, the fascin mutant networks characterized here demonstrate the extremely high variability nature has installed in the viscoelastic response of cytoskeletal networks by making use of actin cross-linking proteins whose local amino acid sequence directly mediates both structural and mechanical features of the networks formed by them.

The authors thank Monika Rusp for the actin preparation and Mireille Claessens for helpful discussions and valuable suggestions on the manuscript. This project was supported by the DFG via SFB 863, project B1 and B11. CH acknowledges the support of the German Science Foundation (DFG) via the Emmy Noether fellowship He 6322/1-1, as well as via SFB 937, project A16. KWM acknowledges the support by the International Graduate School of Science and Engineering (IGSSE), TUM.

Author contribution statement

All authors contributed to the conception and design of the experiments. SK and MM generated the fascin mutants, MM performed the experiments and KWM the simulations. CH contributed the theoretical calculations, and OL, CH, MM and KWM wrote the paper, which was critically revised and approved by all authors.

References

1. A.J. Ridley, Cell **145**, 1012 (2011).
2. D.A. Head, A.J. Levine, F.C. MacKintosh, Phys. Rev. E **68**, 061907 (2003).
3. K.E. Kasza, A.C. Rowat, J.Y. Liu, T.E. Angelini, C.P. Brangwynne *et al.*, Curr. Opin. Cell Biol. **19**, 101 (2007).
4. K.E. Kasza, G.H. Koenderink, Y.C. Lin, C.P. Broedersz, W. Messner *et al.*, Phys. Rev. E **79**, 041928 (2009).
5. O. Lieleg, M.M.A.E. Claessens, A.R. Bausch, Soft Matter **6**, 218 (2010).
6. J.M. Tse, G. Cheng, J.A. Tyrrell, S.A. Wilcox-Adelman, Y. Boucher *et al.*, Proc. Natl. Acad. Sci. U.S.A. **109**, 911 (2012).
7. J. Faix, K. Rottner, Curr. Opin. Cell Biol. **18**, 18 (2006).
8. P.K. Mattila, P. Lappalainen, Nat. Rev. Mol. Cell Biology **9**, 446 (2008).
9. M. Claessens, M. Bathe, E. Frey, A.R. Bausch, Nat. Mater. **5**, 748 (2006).
10. M. Claessens, C. Semmrich, L. Ramos, A.R. Bausch, Proc. Natl. Acad. Sci. U.S.A. **105**, 8819 (2008).
11. Y.S. Aratyn, T.E. Schaus, E.W. Taylor, G.G. Borisy, Mol. Biol. Cell **18**, 3928 (2007).
12. N. Kureishy, V. Sapountzi, S. Prag, N. Anilkumar, J.C. Adams, BioEssays **24**, 350 (2002).
13. D. Vignjevic, M. Schoumacher, N. Gavert, K.P. Janssen, G. Jih *et al.*, Cancer Res. **67**, 6844 (2007).
14. A. Li, J.C. Dawson, M. Forero-Vargas, H.J. Spence, X.Z. Yu *et al.*, Curr. Biol. **20**, 339 (2010).
15. A.U. Jawhari, A. Buda, M. Jenkins, K. Shehzad, C. Sarraf *et al.*, Am. J. Pathol. **162**, 69 (2003).
16. J. Zanet, A. Jayo, S. Plaza, T. Millard, M. Parsons *et al.*, J. Cell Biol. **197**, 477 (2012).
17. S. Ono, Y. Yamakita, S. Yamashiro, P.T. Matsudaira, J.R. Gnarra *et al.*, J. Biol. Chem. **272**, 2527 (1997).
18. D. Vignjevic, S. Kojima, T. Svitkina, G.G. Borisy, J. Cell Biol. **174**, 863 (2006).
19. S. Jansen, A. Collins, C.S. Yang, G. Rebowski, T. Svitkina *et al.*, J. Biol. Chem. **286**, 30087 (2011).
20. S.Y. Yang, F.K. Huang, J.Y. Huang, S. Chen, J. Jakoncic *et al.*, J. Biol. Chem. **288**, 274 (2013).
21. J.A. Spudich, S. Watt, J. Biol. Chem. **246**, 4866 (1971).
22. D. Vignjevic, D. Yarar, M.D. Welch, J. Peloquin, T. Svitkina *et al.*, J. Cell Biol. **160**, 951 (2003).
23. C. Semmrich, R.J. Larsen, A.R. Bausch, Soft Matter **4**, 1675 (2008).
24. C.J. Cyron, W.A. Wall, Int. J. Num. Meth. Engin. **90**, 955 (2012).
25. C.J. Cyron, K.W. Müller, A.R. Bausch, W.A. Wall, J. Comput. Phys. **244**, 236 (2013).
26. C.J. Cyron, K.W. Müller, K.M. Schmoller, A.R. Bausch, W.A. Wall *et al.*, EPL **102**, 38003 (2013).
27. K.W. Muller, R.F. Bruinsma, O. Lieleg, A.R. Bausch, W.A. Wall *et al.*, Phys. Rev. Lett. **112**, 238102 (2014).
28. C.J. Cyron, W.A. Wall, Phys. Rev. E **80**, 066704 (2009).
29. C.J. Cyron, W.A. Wall, Phys. Rev. E **82**, 066705 (2010).
30. G.I. Bell, Science **200**, 618 (1978).
31. O. Lieleg, M. Claessens, C. Heussinger, E. Frey, A.R. Bausch, Phys. Rev. Lett. **99**, 088102 (2007).
32. O. Lieleg, A.R. Bausch, Phys. Rev. Lett. **99**, 158105 (2007).
33. R. Tharmann, M. Claessens, A.R. Bausch, Phys. Rev. Lett. **98**, 088103 (2007).
34. O. Lieleg, K.M. Schmoller, M.M.A.E. Claessens, A.R. Bausch, Biophys. J. **96**, 4725 (2009).
35. C. Heussinger, M. Bathe, E. Frey, Phys. Rev. Lett. **99**, 048101 (2007).
36. L. Wolff, K. Kroy, Phys. Rev. E **86**, 040901 (2012).
37. L. Wolff, P. Fernandez, K. Kroy, Plos One **7**, e40063 (2012).
38. C. Heussinger, New J. Phys. **14**, 095029 (2012).
39. C. Heussinger, E. Frey, Phys. Rev. Lett. **97**, 105501 (2006).
40. S.M. Ward, A. Weins, M.R. Pollak, D.A. Weitz, Biophys. J. **95**, 4915 (2008).